A photochromic metallacycle with highly anisotropic Dy-F magnetic units

Nour El Beyrouti,[a] Felix Houard,[a] Marie Cordier,[a] Elzbieta Trzop,[b] Stéphane Rigaut,[a] Boris Le Guennic,[a] Kevin Bernot[a] and Lucie Norel*[a]

a) Univ Rennes, INSA Rennes, CNRS, ISCR (Institut des Sciences Chimiques de Rennes) – UMR 6226, F-35000 Rennes, France.
b) Univ Rennes, CNRS, IPR (Institut de Physique de Rennes) – UMR 6251, F-35000 Rennes, France.

Electronic Supplementary Information

Contents

1. Synthesis

General comments: The syntheses of the complexes were performed in air. Elemental analyses were obtained on a Thermo Fisher FLASH 1112 instrument at the Centre Régional de Mesures Physiques de l'Ouest. High-resolution mass spectrometry analysis was performed at the Centre Régional de Mesures Physiques de l'Ouest. NMR experiments were performed using a Bruker Avance 400 spectrometer. Compound $[Dy(T_p^{py})F(pyridine)_2]PF_6$ was obtained as previously reported.[1]

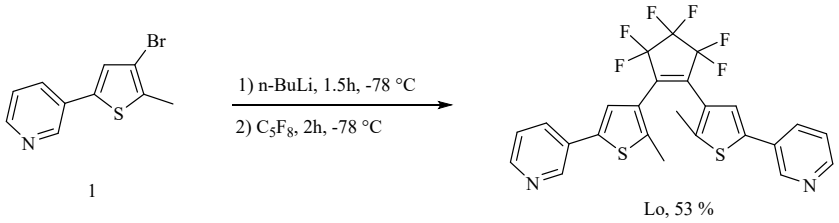

Scheme S1 : Synthesis of compound L_o

Synthesis of L_o: Ligand $\mathbf{L_o}$ was prepared according to a published procedure.[2]

Into a dried schlenck, pure sample of compound 1 (0.505 g, 1.987 x 10^{-3} mol, 2 eq) was introduced under argon. Compound 1 was dissolved by 20 mL of dry diethylether, and the mixture was cooled down to -78°C. To the mixture, n-BuLi (1 mL, 2.186 x 10^{-4} mol, 2.2 eq) were added dropwise, and the mixture was stirred for 1.5 h at -78 °C. Through cannula transfer, a cold solution of perfluorocyclopentene (0.135 mL, 9.935 x 10^{-4} mol, 1 eq) in 2 mL of dry diethylether was added dropwise. The mixture was stirred for 2 h at -78°C, then overnight at room temperature. The mixture was washed with water (25 mL), and the crude compound was extracted by diethylether (3 x 20 mL). The organic phase was dried over $MgSO_4$, filtered, and evaporated. The crude compound was purified by silica column chromatography using PE/EtOAc (1:1) as eluent. Compound Lo was obtained as a bight orange solid (53 %).

^{1}H NMR (400 MHz, $CDCl_3$): δ (ppm) = 8.82 (d, *J* = 1.9 Hz, 2H), 8.56 (dd, *J* = 4.8, 1.4 Hz, 2H), 7.83 (ddd, *J* = 8.0, 2.4, 1.6 Hz, 2H), 7.35 – 7.32 (m, 4H), 2.03 (s, 6H). **^{19}F NMR** (376 MHz, $CDCl_3$): δ (ppm) = -110.05 (t, *J* = 5.3 Hz, 4F), -131.85 (quint, *J* = 5.3 Hz, 2F).

Synthesis of L_c: Ligand $\mathbf{L_o}$ (50 mg) was dissolved in dichloromethane (160 mL). The solution was irradiated at 312 nm for 80 min within Rayonet illumination chamber with a power of 4.14 mW·cm^{-2}. The photoconversion was 90 % as estimated by ^{1}H NMR. The dichloromethane was then evaporated under reduced pressure and the resulting blue solid was purified on silica gel column (diethylether) to yield ligand $\mathbf{L_c}$ as a blue powder. The ^{1}H NMR spectrum of $\mathbf{L_c}$ matches previously published data and features $\mathbf{L_o}$ in small amounts (4 %).

^{1}H NMR (400 MHz, $CDCl_3$): δ (ppm) = 8.85 (d, *J* = 2.4 Hz, 2H), 8.67 (dd, *J* = 4.8, 1.6 Hz, 2H), 7.87 (dt, *J* = 8.1, 2.0 Hz, 2H), 7.40 (dd, *J* = 8.1, 4.8 Hz, 2H), 6.76 (s, 2H), 2.23 (s, 6H). **^{19}F NMR** (376 MHz, $CDCl_3$): δ (ppm) = -111.75 to -114.22 (m, 4F), -133.47 (quint, *J* = 6.9 Hz, 2F).

Synthesis of [$DyT_p^{py}F(pyridine)_2$]BArF:

A solution of compound [$DyT_p^{py}F(pyridine)_2$]PF_6 (0.031 g, 3.385 10^{-5} mol, 1 eq) and sodium tetrakis(3,5-bis(trifluoromethyl)phenyl)borate (0.031 g, 3.385 10^{-5} mol, 1 eq) in dichloromethane (4 ml) was stirred for 24 hours at room temperature. The solution was filtered over a plug of celite to remove the precipitate ($NaPF_6$), and the solvent was removed under reduced pressure. The yield was found to be quantitative. The compound was crystallized by slow diffusion of n-pentane to a solution of the compound in dichloromethane. Colorless stick crystals were isolated after 1-2 nights and solved by single XRD analysis.

FT-IR spectroscopy (cm^{-1}): 2494, 1610, 1596, 1494, 1436, 1389, 1354, 1273, 1193, 1157, 1118, 1088, 1058, 1045, 1005, 1003, 891, 886, 839, 801, 794, 770, 758, 713, 682, 666, 636.

Synthesis of [$YT_p^{py}F(pyridine)_2$]BArF:

Similar procedureas **[$DyT_p^{py}F(pyridine)_2$]BArF** using (0.031 g, 3.626 10^{-5} mol, 1 eq) of [$YT_p^{py}F(pyridine)_2$]PF_6 and (0.032 g, 3.626 10^{-5} mol, 1 eq) of NaBArF. The yield was found to be quantitative. Crystallization was performed in the same way as the dysprosium complex .

FT-IR spectroscopy (cm^{-1}): 2492, 1608, 1599, 1494, 1437, 1389, 1354, 1275, 1187, 1144, 1127, 1112, 1090, 1072, 1052, 1036, 1005, 897, 885, 838, 799, 772, 767,702 665. **^{1}H NMR** (400 MHz, $CDCl_3$): δ (ppm) = 9.30 (d, *J* = 5.3 Hz, 3H), 8.53 (dd, *J* = 4.4, 1.6 Hz, 4H), 7.95 (dt, *J* = 7.6, 1.6 Hz, 4H), 7.89 (d, *J* = 2 Hz, 3H), 7.85 (br-s, 2H), 7.83 (br-s, 2H), 7.58 (s, 12H), 7.51- 7.46 (m, 3H), 7.45 – 7.41 (m, 4H), 6.76 (d, *J* = 2.3 Hz, 3H). **^{19}F NMR** (376 MHz, $CDCl_3$): δ (ppm) = -38.28 (d, *J* = 71.44 Hz, Y-F), -64.31 (S, C-F of BArF).

Synthesis of 1c: [$Dy(T_p^{py})F(pyridine)_2$]BArF (0.016 g, 9.716 10^{-6} mol, 1 eq) and compound $\mathbf{L_c}$ (0.0153 g, 2.91 10^{-5} mol, 3 eq) were dissolved in a mixture of 4 ml of dichloromethane and hexane (1:1). Blue prisms crystals were obtained after storage overnight. The crystals were isolated via filtration of the remaining solution, rinsed with hexane, and air-dried in the dark (0.0157 g, 7.73 10^{-6} mol, 79 %).

FT-IR spectroscopy (cm^{-1}): 2492, 1634, 1591, 1494, 1430, 1358, 1277, 1192, 1164, 1126, 1094, 1050, 971, 877, 706, 677. **Elemental analysis**: Calcd for $C_{162}H_{94}N_{22}F_{62}B_4S_4Dy_2.4C_5H_{12}$: H, 3.32; C, 50.70; N, 7.15; S, 2.97, Found H, 3.44; C, 53.01; N, 6.32; S, 3.87. **HR-MS**: only fragments were detected such as the one corresponding to [$DyT_p^{py}F(L_c)$]$^+$, *m/z* calcd. for [$C_{49}H_{35}N_{11}F_7{}^{11}BS_2{}^{164}Dy$]$^+$: 1149.1786, found: 1149.1791.

Synthesis of 2c:

Similarly for **2c** using (0.018 g, 1.14 10^{-5} mol, 1 eq) of [Y(T_p^{py})F(pyridine)$_2$]BArF and compound $\mathbf{L_c}$ (0.018 g, 3.43 10^{-5} mol, 3 eq). 73 % yield (0.016 g of crystals of 2c, 8.174 x 10^{-6} mol)

FT-IR spectroscopy (cm^{-1}): 2487, 1607, 1634, 1493, 1353, 1272, 1192, 1163, 1120, 1093, 1046, 978, 888, 877, 767, 706, 681, 670. **^{1}H NMR** (400 MHz, CD_3OD): δ (ppm) = 9.31 (d, *J* = 5.3 Hz, 3H), 8.84 (d, *J* = 2.7 Hz, 2H), 8.61 (dd, *J* = 4, 1.6 Hz, 2H), 8.13 (td, *J* = 8, 1.6 Hz, 2H), 7.95 (td, *J* = 7.6, 1.7 Hz, 4H), 7.89 (d, *J* = 2.3 Hz, 3H), 7.85 (br-s, 2H), 7.83 (br-s, 2H), 7.58 (s, 12H), 7.56 - 7.55 (m, 3H), 7.51 - 7.46 (m, 4H), 6.99 (s, 3H), 6.76 (d, *J* = 2.4 Hz, 3H), 2.24 (s, 6H).**^{19}F NMR** (376 MHz, CD_3OD): δ (ppm) = - 38.26 (d, *J* = 69.8 Hz, Y-F), - 64.31 (S, C-F of BArF), -114.65 (m, 4F), -135.40 (quint, *J* = 5.6 Hz, 2F). In these conditions, **2c** is dissociated and the NMR shows [$\mathbf{DyT_p^{py}F(CD_3OD)_2}$] and free $\mathbf{L_c}$.

Preparation of 1o: Crystals of $\mathbf{1_c}$ were placed in paratone oil and irradiated for 5h using a laser (power = 2.5 mW, λ = 666 nm), resulting in pale violet crystals of $\mathbf{1_o}$. We note that some of the crystals fractured over the course of irradiation.

FT-IR spectroscopy (cm^{-1}): 2493, 1606, 1495, 1435, 1354, 1279, 1194, 1147, 1126, 1055, 987, 888, 839, 798, 776, 716, 682, 543.

2. Single Crystal XRD

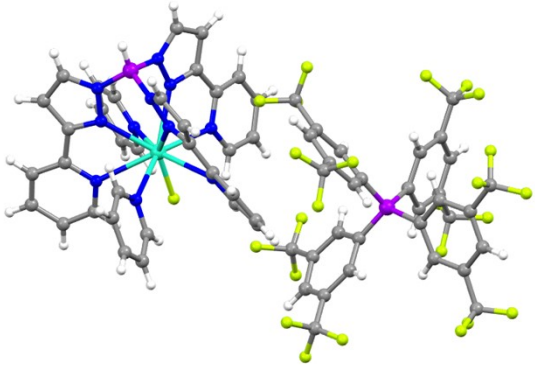

Figure S1. View of the structure of [Dy(T_p^{py})F(pyridine)$_2$]BArF.

Table S1. Crystallographic data on the structure of [Dy(T_p^{py})F(pyridine)$_2$]BArF.

	[DyT_p^{py}F(pyridine)$_2$](BArF)
CCDC deposition number	2239099
T (K)	150
Space group	monoclinic, $P\,2_1/c$
a, b, c (Å)	17.8820(9), 22.3642(8), 16.6012(7)
β (°)	91.536(2)
Volume (Å^3)	6636.7(5)
Z	4
Calculated density	1.649 g.cm^{-3}
R [I>2σ]	0.0411
R(all indices)	0.0802

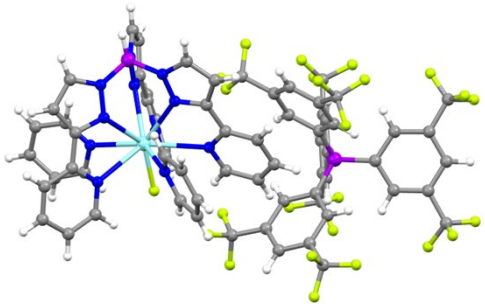

Figure S2. View of the structure of [Y(T_p^{py})F(pyridine)$_2$]BArF.

Table S2. Crystallographic data on the structure of [Y(T_p^{py})F(pyridine)$_2$]BArF.

	[YT_p^{py}F(pyridine)$_2$](BArF)
CCDC deposition number	2239100
T (K)	150
Space group	monoclinic, $P\,2_1/c$
a, b, c (Å)	17.8660(7), 22.3348(8), 16.6191(6)
β (°)	91.516(2)
Volume (Å^3)	6629.3(4)
Z	4
Calculated density	1.577 g.cm^{-3}
R [I>2σ]	0.0487
R(all indices)	0.1036

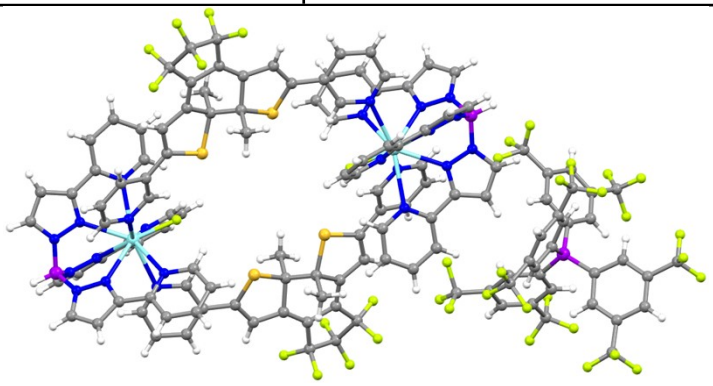

Figure S3. View of the structure of **2c**.

Table S3. Selected crystallographic data of structure of **1c** and **2c**.

	1c	**2c**
CCDC deposition number	2207245	2207246
T (K)	150 K	150 K
Space group	triclinic, P -1	triclinic, P -1
a, b, c (Å)	16.4364(9), 16.9248(11), 17.7462(11)	16.4627(9), 16.8932(10), 17.7103(10)
α, β, γ (°)	85.374(2), 66.379(2), 67.884(2) °	85.238(2), 66.519(2), 68.042(2)
Volume (Å^3)	4175.9	4177.18
Z,	1	1
Calculated density	1.600 g.cm^{-3}	1.555 g.cm^{-3}
R [I>2σ]	0.0504	0.0623
R(all indices)	0.0845	0.1763

Table S4: Crystallographic data of structure of compound **1o**.

	1o
CCDC number	2221723
T	90 K
Space group	triclinic, P -1
a, b, c (Å)	16.7214(14), 17.9382(11), 17.1947(12)
α, β, γ (°)	84.845(5), 66,873(7), 63.672(7)
Volume (Å^3)	4228,78
Z	1
Calculated density	1.575 g.cm^{-3}
R [I>2σ]	0.063
R(all indices)	0.1189

Details about the structure of 1o: Photo-induced **1o** form was obtained after irradiation of several single crystals with 660 nm at 2.5 mW laser power. After six and a half hours of irradiation, clear color change from dark blue to dark violet have been observed. Out of the whole crystals batch, one single crystal was selected for full data collection at 90 K. Data for **Dy-1o** were collected on an Xcalibur 3 four-circle diffractometer (Oxford Diffraction) equipped with a 2D Sapphire3 CCD detector, a Mo-Kα radiation source (λ = 0.71073 Å, graphite monochromator) and an Oxford Cryosystems nitrogen-flow 700 cryostat. Data collection and data reduction were performed by the means of CrysAlisPro[3] software from Rigaku Oxford Diffraction. Under Olex2 GUI,[4] the structure was solved by dual-space algorithm using the *SHELXT* program,[5] and then refined with full-matrix least-squares methods based on F^2 (*SHELXL*) [6] The contribution of the disordered solvents to the calculated structure factors was estimated following the *BYPASS* algorithm[7], implemented as the *SQUEEZE* option in *PLATON*.[8] All non-hydrogen atoms were refined with anisotropic atomic displacement parameters and H-atoms were constrained by geometry. When necessary, DANG, SADI, SIMU and ISOR restrains were applied for occupational disorder. The crystal data collection and refinement parameters are given in table **S4.**

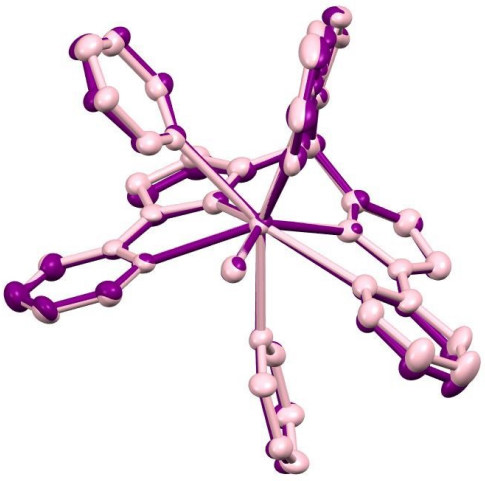

Figure S4. Overlay of the coordination spheres of the Dysprosium centers for **1c** (purple) and **1o** (pink).

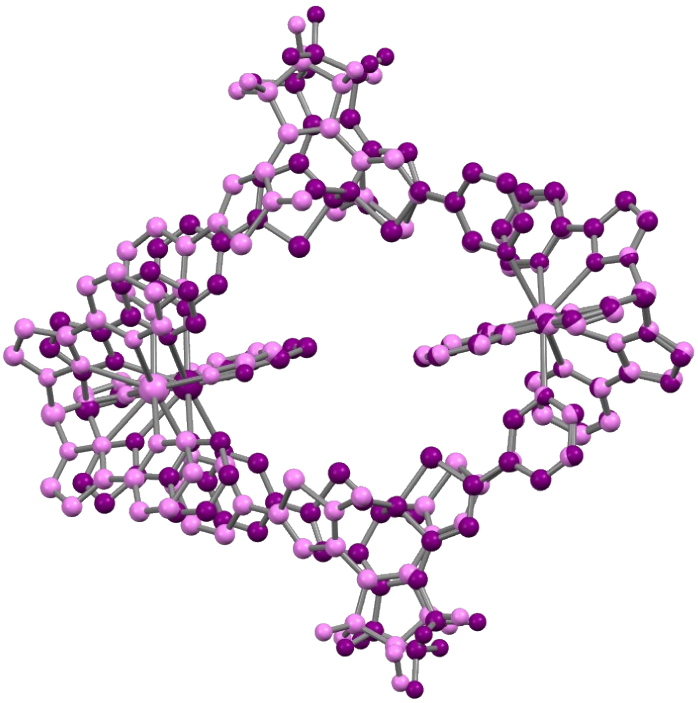

Figure S5. Total overlay of the ring structures of **1c** (purple) and **1o** (pink).

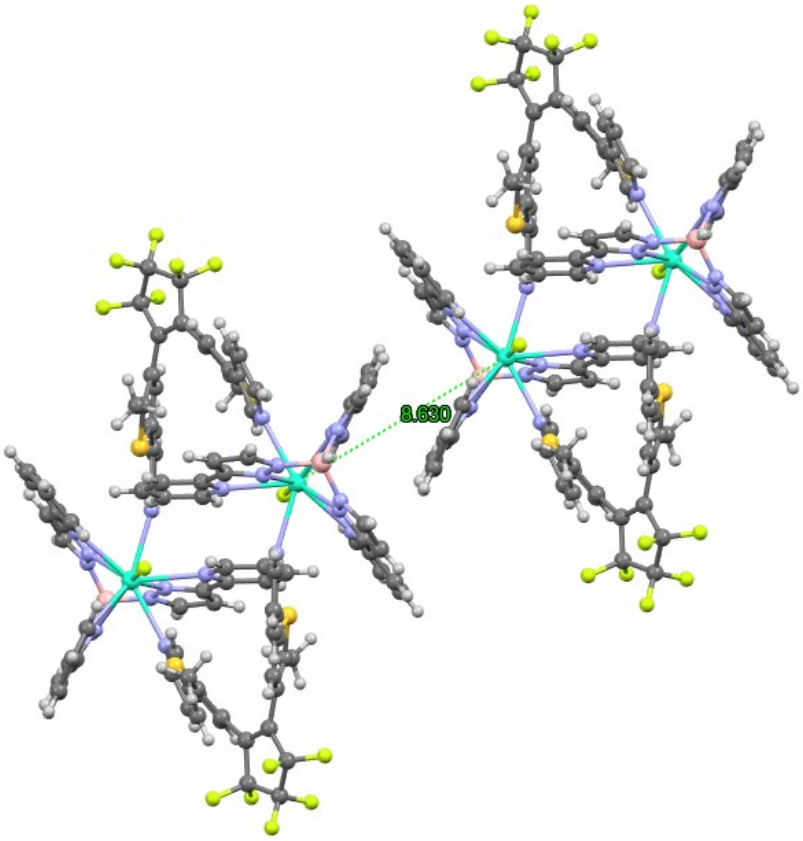

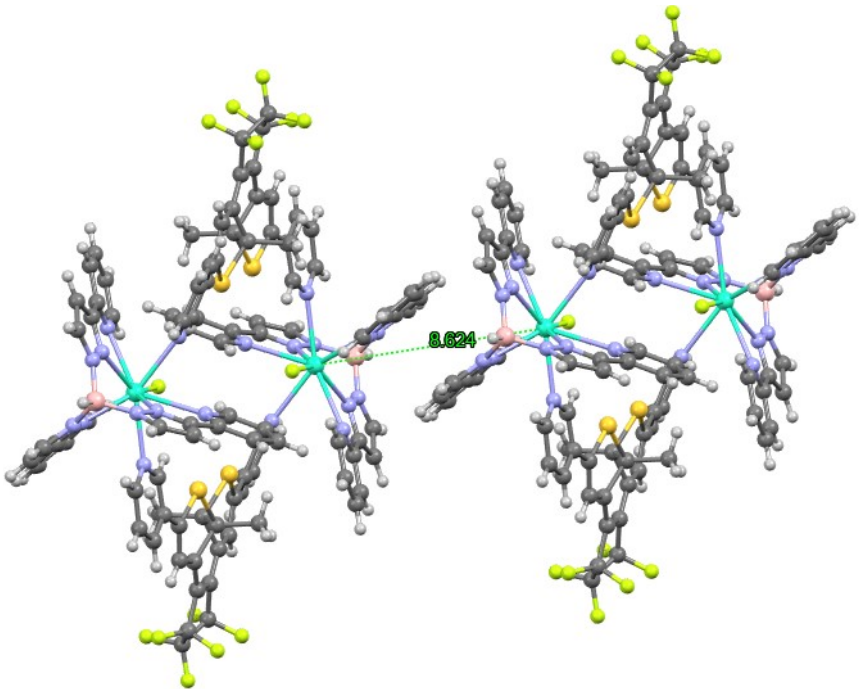

Figure S6. Comparison of the packing between **1o** (top view) and **1c** (bottom view)

3. Isomerization

The absorption measurements were performed in CH_2Cl_2 and KBr pellet at room temperature using “UV VIS NIR JASCO” spectrometer. Routine UV-vis irradiations were performed in UV cells with UV lamp at λ = 365 nm (TLC lamp) for closing reaction, and with a Xenon lamp (with a filter at λ = 580 nm) or white low power LED lamp for the opening reaction.

^{1}H NMR and ^{19}F NMR spectra were recorded using Bruker Avance 400 (400 MHz). Sample for NMR measurements were irradiated with Rayonet irradiation chamber at λ = 313 nm for the closing reaction, and white light for the opening reaction.

Figure S7. Electronic absorption spectra of $\mathbf{L_o}$ in KBr pellet before irradiation (dark blue) and after UV light irradiation at 365 nm for 10, 30, 60, 100, 150, 210, 300 seconds until reaching the photostationary state (light blue), followed with white light until reaching the initial state in 27 minutes (dashed red).

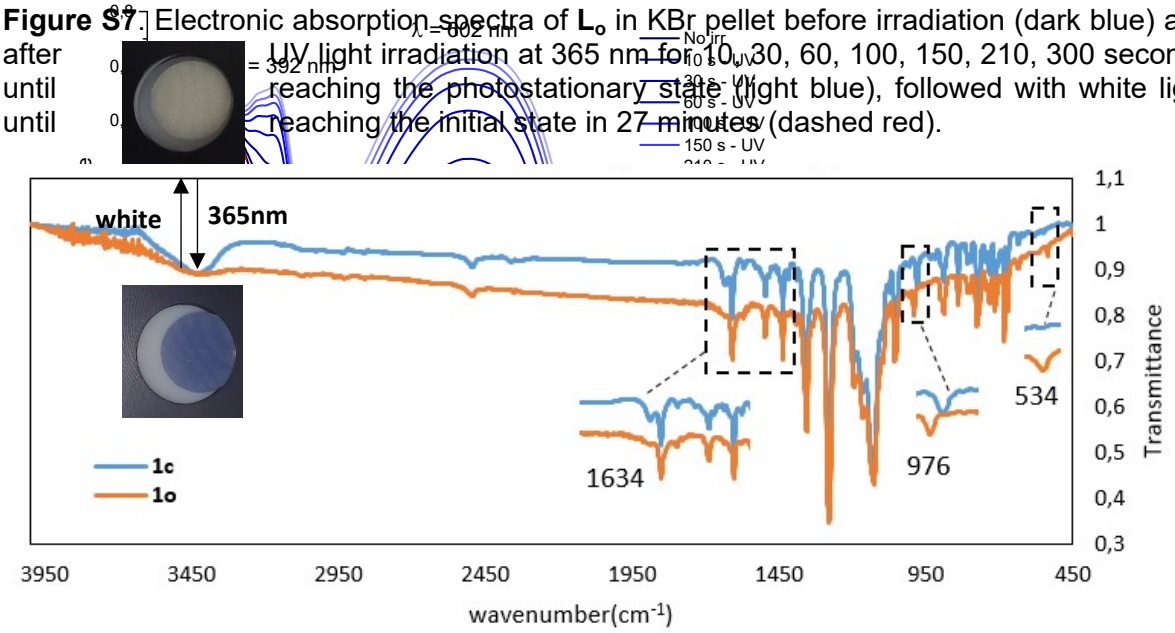

Figure S8. IR spectra of compound **1c** before and after white light irradiation leading to **1o**.

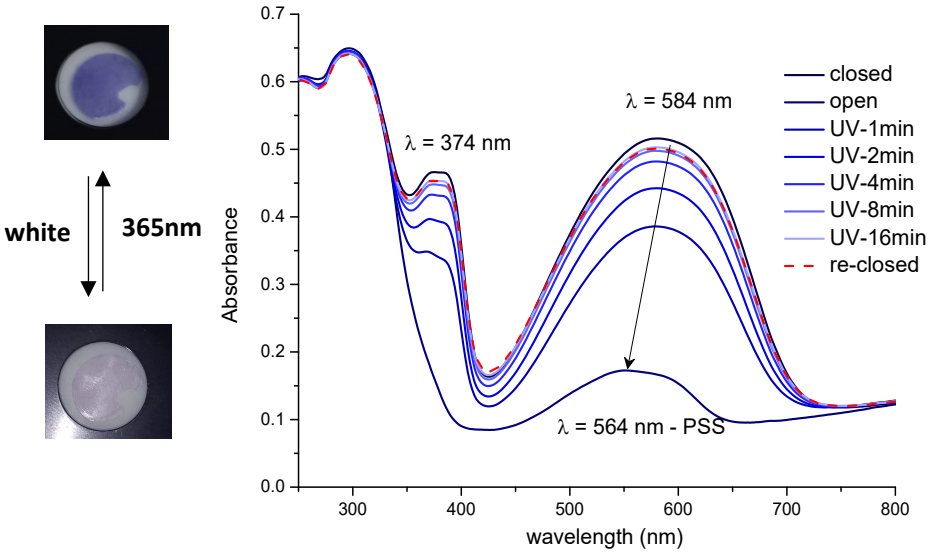

Figure S9. Electronic absorption spectra of **1c** in KBr pellet upon irradiation with white light for 35 minutes until reaching the PSS, followed with UV light irradiation at λ = 365 nm until reaching the initial spectrum (32 minutes, dashed red).

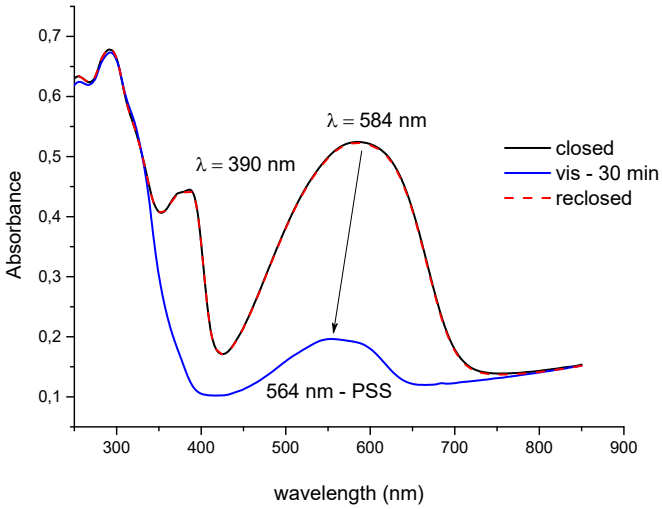

Figure S10. Electronic absorption spectra of **2c** in KBr pellet before and after irradiation with white light for 30 minutes until reaching the photostationary state, and with UV light at λ = 365 nm until reaching the initial spectra (dashed red).

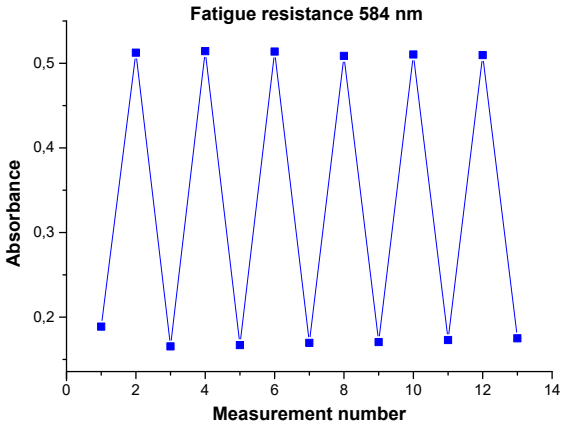

Figure S11. Absorbance recorded at 584 nm on **1o** in KBr pellet, after 32 min of UV light irradiation (λ = 365 nm) followed by 35 minutes of white light irradiation, and then after five identical cycles of irradiation.

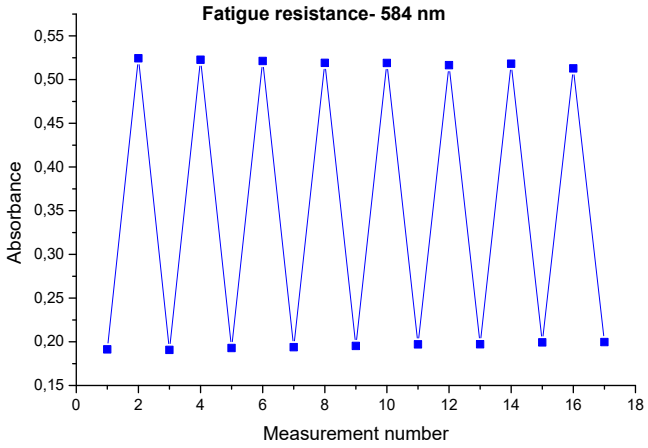

Figure S12. Absorbance recorded at 584 nm for **2o** in KBr pellet, after 19 min of UV light irradiation (λ = 365 nm) followed by 30 minutes of white light irradiation, and then after seven identical cycles of irradiation.

Following of the photoisomerization by solution NMR spectroscopy

^{1}H NMR spectrum of **2c** in d^2-dichloromethane is not showing the signals of free $\mathbf{L_c}$. It means that the dinuclear structure is at least partly maintained in dichloromethane solution. Upon white light irradiation, the spectrum evolves toward the expected signals for **2o**. Therefore, the study of isomerization by absorption spectroscopy in dichloromethane solution was considered to probe the behavior of the dinuclear compound (Figure S15). On the contrary, when the analysis was performed in CD_3OD, total disassembly of the dinuclear ring to form $\mathbf{[DyT_p^{py}F(CD_3OD)_2]}$ and free L was observed. This provide a way to analyze the exact $\mathbf{L_o}$ to $\mathbf{L_c}$ ratio of any solid batch during the course of its isomerization, as shown in Figure S17-18.

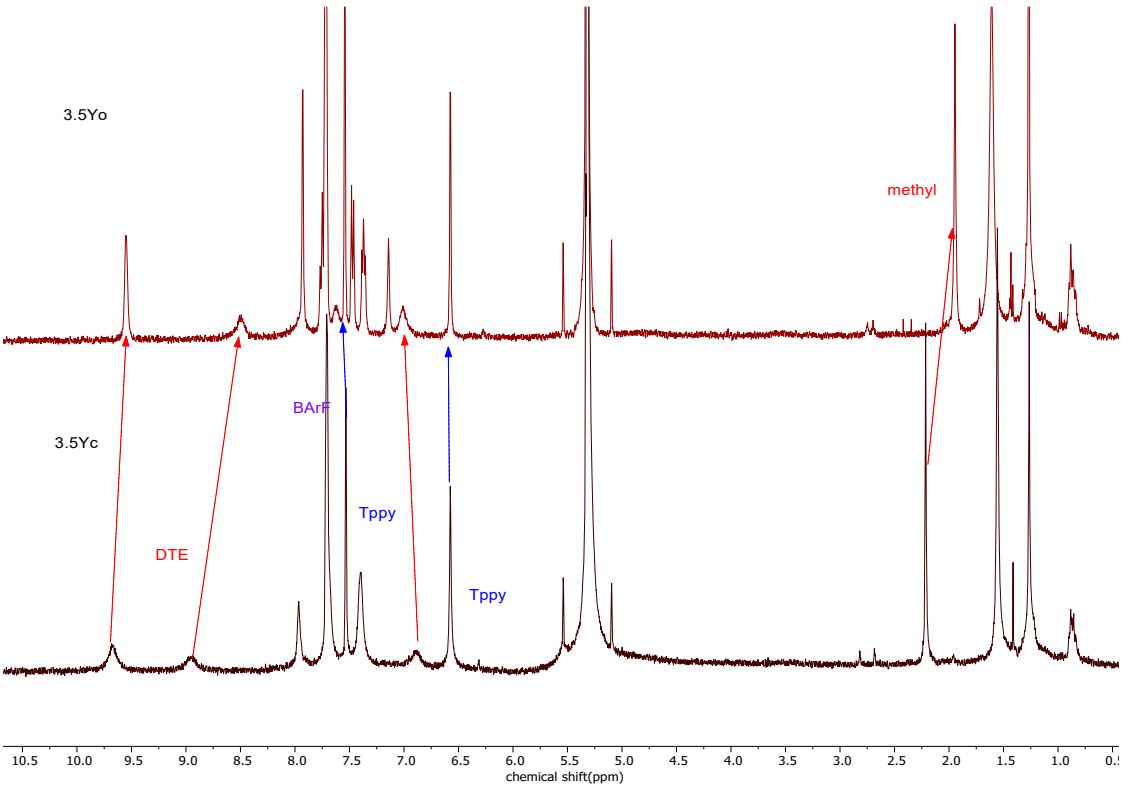

Figure S13. ^{1}H NMR spectra (400 MHz, CD_2Cl_2) of **2c** before and after white light irradiation for 100 minutes.

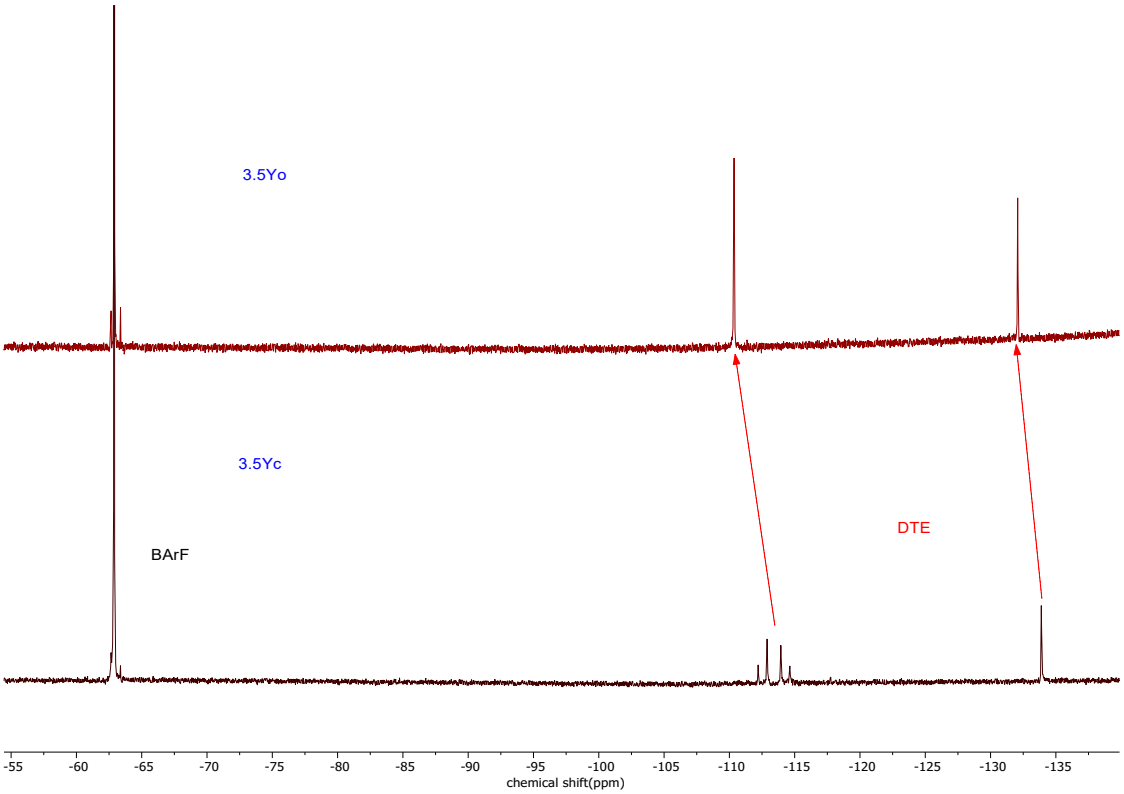

Figure S14. ^{19}F NMR spectra (400 MHz, CD_2Cl_2) of **2c** before and after white light irradiation for 100 minutes.

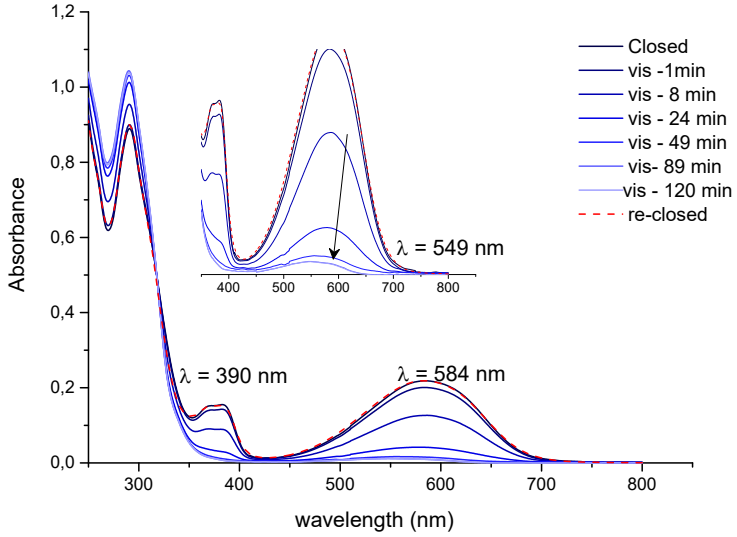

Figure S15. Electronic absorption spectra of **1c** in dichloromethane upon visible light (λ = 530 nm) irradiation for 120 minutes until reaching the photostationary state (from black to light blue), and with UV light at λ = 365 nm until reaching the initial spectra (dashed red).

Following of solid-state isomerization by NMR spectroscopy on 2c

Compound **2c** (crashed crystals) was irradiated with white light for 92 h, resulting in violet solid powder of **2o**. The photostationary state was checked by electronic absorption and it was found to overlay with the measurements in KBr pellet (Figure S16).

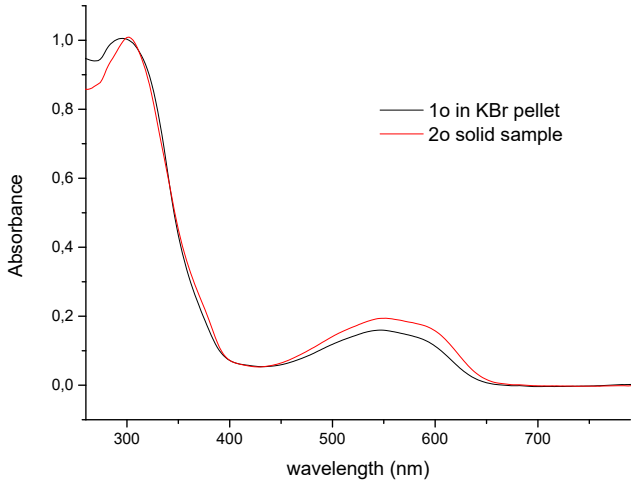

Figure S16. Electronic absorption measurement showing the overlay between the PSS reached in a KBr pellet for **1c** and in the powder sample for **2c**.

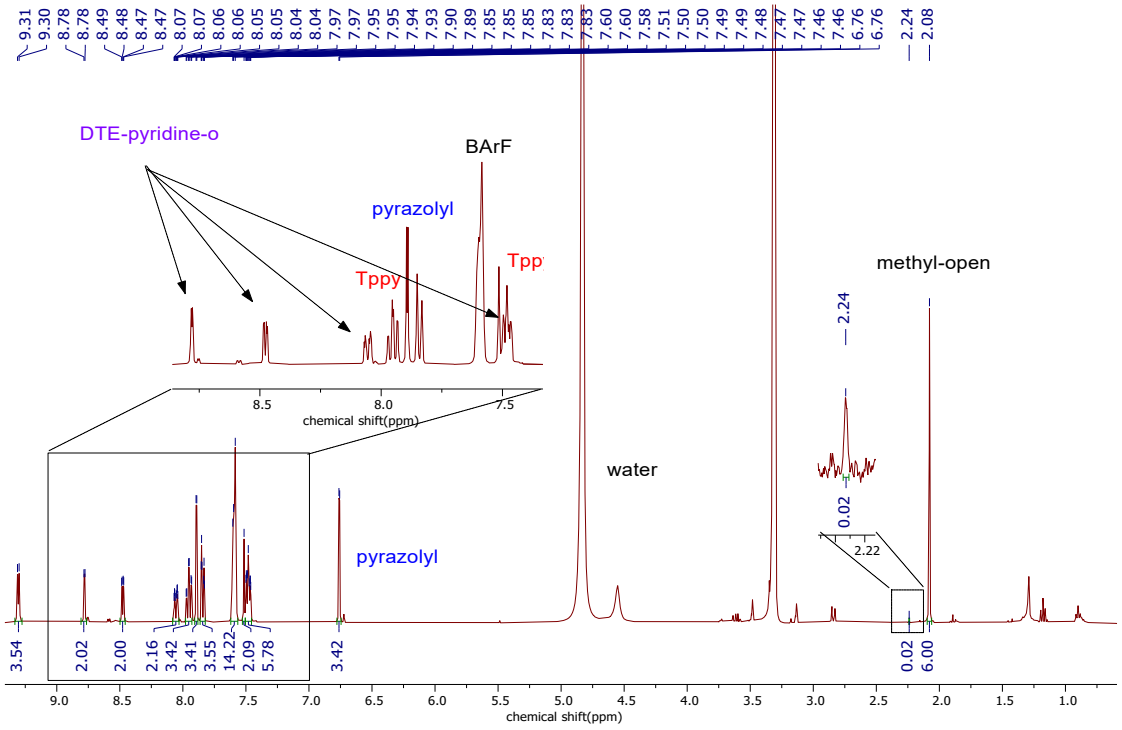

Figure S17. ^{1}H NMR spectrum of **2o** (400 MHz, CD_3OD) generated by irradiation of the solid crystalline powder of **2c** and showing a ratio of $\mathbf{L_o}$ to $\mathbf{L_c}$ of 6 to 0.02.

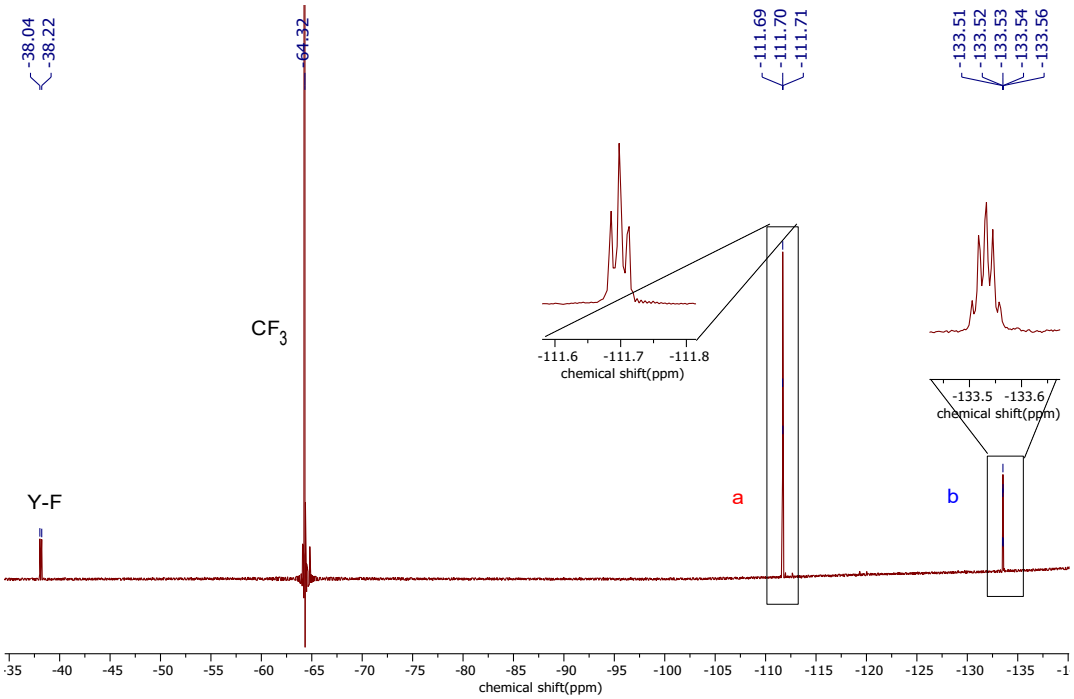

Figure S18. ^{19}F NMR spectrum of **2o** (376 MHz, CD_3OD) generated by irradiation of the solid crystalline powder of **2c** and showing only $\mathbf{L_o}$.

4. Magnetic Characterization

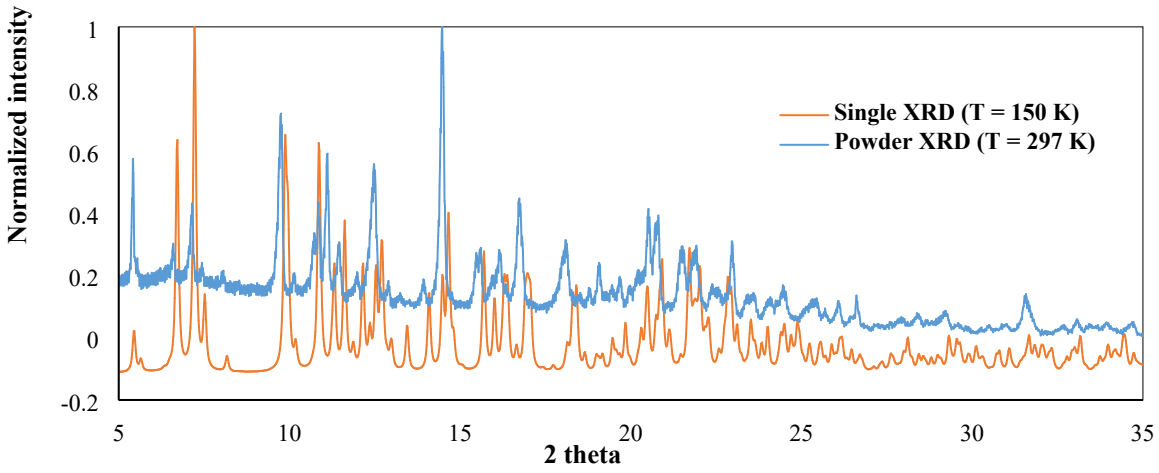

Figure S19. Powder XRD pattern and data from single XRD for compound **1c**.

Preparation of 1o for powder XRD analysis and magnetic measurements: Compound **1c** (crashed crystals) was irradiated with white light for 88 h, resulting in violet solid powder of **1o**. The photostationary state was checked by electronic absorption and it was found to overlay with the measurements in KBr pellet (Figure S21).

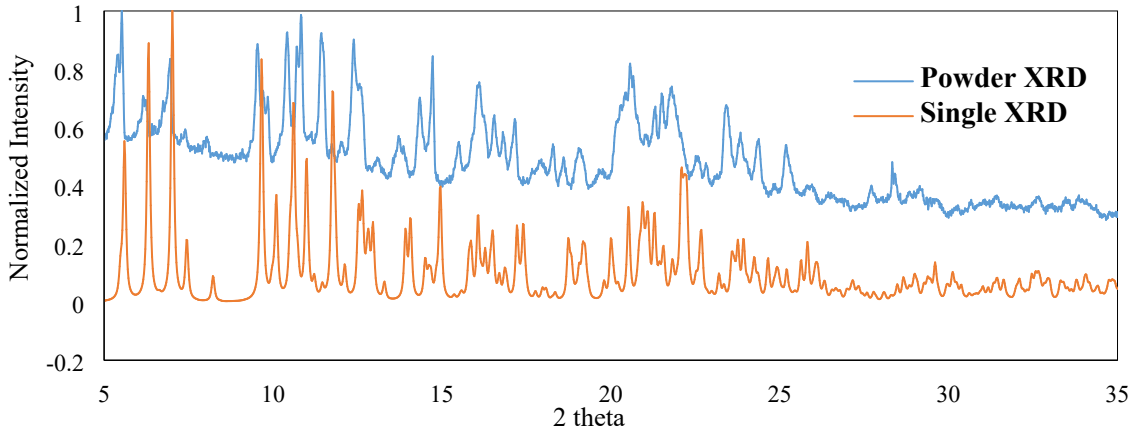

Figure S20. Powder XRD pattern and data from single XRD for compound **1o**.

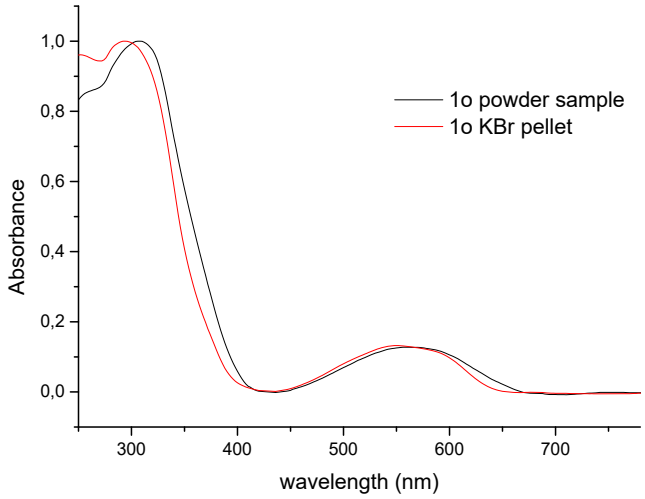

Figure S21. Absorption spectrum of the irradiated powder sample of **1c** (black) in comparison to the PSS reached in KBr pellet (red).

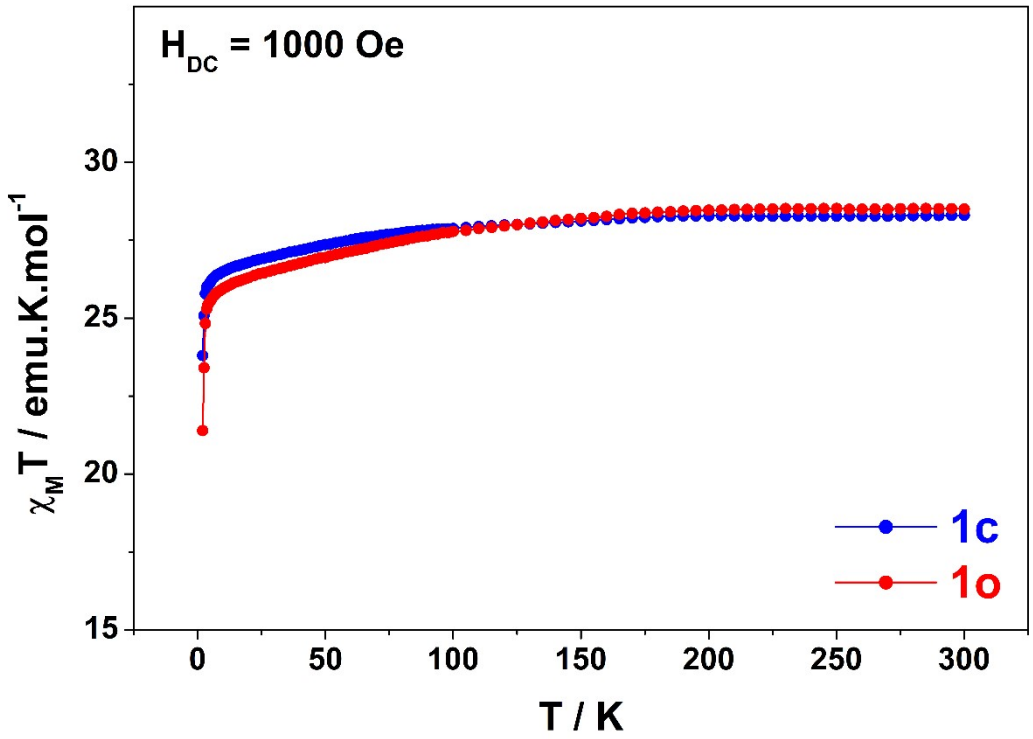

Figure S22. Temperature dependence of the molar magnetic susceptibility times temperature ($\chi_M T$) for **1c** (blue) and **1o** (red) collected under H_{DC} = 1000 Oe.

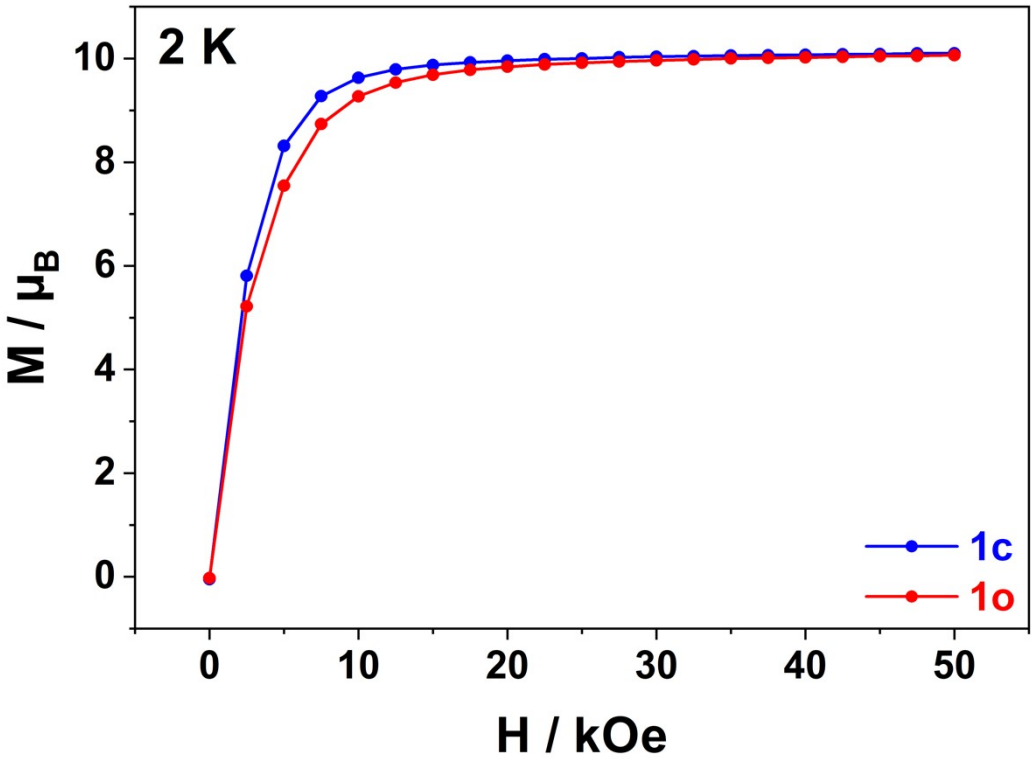

Figure S23. Magnetization curves for **1c** (blue) and **1o** (red) at 2 K.

Table S5. Relaxation times for **1c** extracted from fitting out-of-phase magnetic susceptibility data collected at H_{DC} = 0 Oe (H_{AC} = 3 Oe).

T (K)	*τ (μs)*
2	140079
4	72434
6	51307
8	32344
10	19868
12	12527
14	8338
16	5895
18	4290
20	3253
22	2483
24	1909
26	1469
28	1124
30	864
32	678
34	507
36	399
40	211
42	158
44	110
46	69

Table S6. Parameters extracted from fits of the in- and out-of-phase magnetic susceptibility data for **1c**, H_{DC} = 0 Oe (H_{AC} = 3 Oe) using a generalized Debye model.

T (K)	χ_S *(emu.mol^{-1})*	χ_T *(emu.mol^{-1})*	*α*	R^2
2	0.33613	14.83053	0.39321	0.99979
4	0.23935	6.86559	0.34946	0.99886
6	0.19776	4.54452	0.32238	0.99824
8	0.1914	3.30842	0.27054	0.99686
10	0.17823	2.59095	0.21719	0.99135
12	0.17188	2.12446	0.1775	0.98791
14	0.16273	1.81825	0.14544	0.9897
16	0.15196	1.60058	0.12869	0.98757
18	0.15791	1.42622	0.10115	0.99215
20	0.15369	1.29405	0.0944	0.98788
22	0.14201	1.18621	0.09889	0.98058
24	0.12776	1.09774	0.10285	0.97125
26	0.13399	1.02133	0.09608	0.98602
28	0.14081	0.95389	0.07935	0.98611
30	0.12986	0.89715	0.09169	0.96732
32	0.15268	0.8356	0.06592	0.92814
34	0.15289	0.80542	0.08421	0.98646
36	0.17876	0.7624	0.02796	0.97425

Table S7. Relaxation times for **1c** extracted from fitting out-of-phase magnetic susceptibility data collected under H_{DC} = 1600 Oe (H_{AC} = 3 Oe).

T (K)	*τ (μs)*
10	97633
12	43901
14	24206
16	14670
18	9590
20	6512
22	4530
24	3198
26	2268
28	1604
30	1197
32	824
34	623
36	470
38	342
40	248
42	162
44	118
46	81

Table S8. Parameters extracted from fits of the in- and out-of-phase magnetic susceptibility data for **1c** (H_{AC} = 3 Oe, H_{DC} = 1600 Oe) using a generalized Debye model.

T (K)	χ_S *(emu.mol^{-1})*	χ_T *(emu.mol^{-1})*	*α*	R^2
10	0.12555	2.54966	0.09783	0.99667
12	0.12183	2.11061	0.08664	0.99819
14	0.10355	1.83559	0.11042	0.99029
16	0.101	1.59977	0.08492	0.99503
18	0.10291	1.4267	0.08601	0.9946
20	0.09675	1.28918	0.08651	0.98891
22	0.10035	1.17841	0.07679	0.97854
24	0.10045	1.08562	0.07666	0.98767
26	0.08736	1.00925	0.08672	0.98045
28	0.08425	0.94391	0.10008	0.9816
30	0.09441	0.88343	0.08742	0.9737
32	0.09875	0.83246	0.07293	0.97594
34	0.12231	0.78745	0.05956	0.97258
36	0.14735	0.7468	0.0553	0.97261

Table S9. Relaxation times for **1o** measured under H_{DC} = 0 Oe (H_{AC} = 3 Oe).

T (K)	*τ (μs)*
2	494863
4	351519
6	202006
8	76747
10	37346
12	21161
14	13581
16	9141
18	6277
20	4651
22	3399
24	2616
26	1980
28	1477
30	1097
32	849
34	653
36	460
38	325
40	206
42	122
44	47

Table S10. Parameters extracted from fits of the in- and out-of-phase magnetic susceptibility data for **1o** (H_{AC} = 3 Oe, H_{DC} = 0 Oe) using a generalized Debye model.

T (K)	χ_S *(emu.mol^{-1})*	χ_T *(emu.mol^{-1})*	*α*	R^2
2	0.13759	17.07899	0.47151	0.99985
4	0.12352	8.45615	0.43282	0.99983
6	0.11376	5.4337	0.37829	0.99946
8	0.12012	3.69911	0.29128	0.99713
10	0.11632	2.75019	0.20919	0.99066
12	0.10718	2.20268	0.15248	0.98446
14	0.10456	1.87008	0.10997	0.9865
16	0.08868	1.63815	0.10475	0.97931
18	0.09997	1.45401	0.06062	0.98386
20	0.09546	1.31424	0.05536	0.99008
22	0.09308	1.19756	0.04488	0.99142
24	0.09187	1.10688	0.04349	0.9912
26	0.0968	1.02517	0.02105	0.98561
28	0.09775	0.95651	0.02322	0.99254
30	0.08186	0.90159	0.05964	0.97591
32	0.09205	0.84875	0.02995	0.99034
34	0.10114	0.80595	0.02502	0.85146
36	0.10019	0.76583	0.01092	0.99195
38	0.11867	0.7294	0.00406	0.98462
40	0.11049	0.68789	4.14764E-16	0.92752

Table S11. Extracted relaxation times for **1o** measured under H_{DC} = 1600 Oe.

T (K)	*τ (μs)*
8	353025
10	122147
12	52582
14	28386
16	16755
18	10536
20	7473
22	5129
24	3694
26	2632
28	1924
30	1386
32	1011
34	745
36	517
38	353
40	226
42	132
44	81
46	55

Table S12. Parameters extracted from fits of the in- and out-of-phase magnetic susceptibility data for **1o** (H_{AC} = 3 Oe, H_{DC} = 1600 Oe) using a generalized Debye model.

T (K)	χ_S *(emu.mol^{-1})*	χ_T *(emu.mol^{-1})*	*α*	R^2
8	0.07948	3.30399	0.05978	0.99375
10	0.08116	2.52999	0.03296	0.9942
12	0.06145	2.11952	0.04425	0.99195
14	0.05639	1.82762	0.04906	0.99739
16	0.09284	1.58637	0.01276	0.89727
18	0.05416	1.42266	0.03239	0.97959
20	0.05782	1.28551	0.03945	0.97787
22	0.05257	1.1707	0.02747	0.99711
24	0.05046	1.07624	0.03431	0.99109
26	0.05512	0.99981	0.03488	0.97716
28	0.06062	0.92921	0.02309	0.9942
30	0.06288	0.87089	0.02524	0.9959
32	0.06981	0.8003	2E-16	0.90718
34	0.06807	0.76502	0.01045	0.98693
36	0.07208	0.73144	0.00453	0.96547
38	0.06146	0.69688	0.02204	0.98433
40	0.07303	0.66466	0.02862	0.9735

Table S13. Characteristic relaxation values of **1c** and **1o** under H_{DC} = 1600 Oe, extracted from Equation (1) in the main text: $\tau^{-1} = BT^n + \tau_0^{-1}\exp(-U_{eff}/k_BT)$. The Orbach regime was determined on the basis of fits to the linear regime of the Arrhenius plot and values for this process fixed in the comprehensive fitting procedure.

	1c	**1o**
***B* ($s^{-1}·K^{-n}$)**	0.012 (± 0.008)	0.013 (± 0.012)
n	3.06 (± 0.23)	2.94 (± 0.33)
τ_0 (10^{-7} s)	1.86 (± 0.35)	
U_{eff} (cm^{-1})	193 (± 17)	

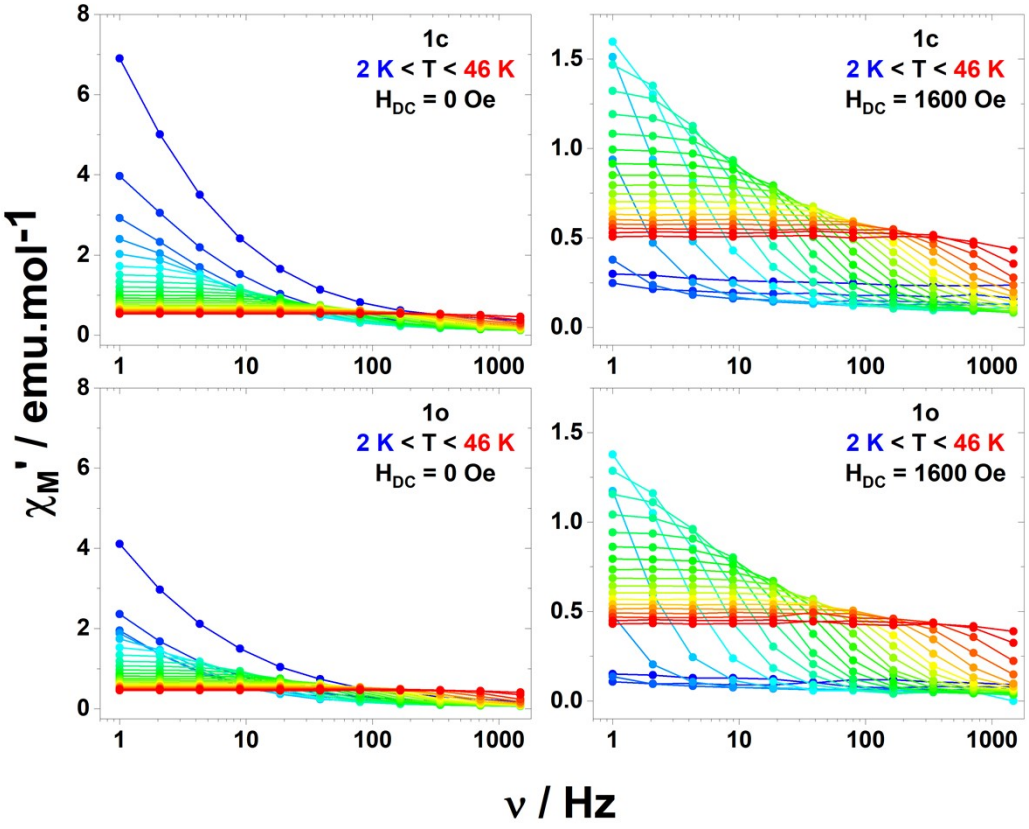

Figure S24. In-phase molar magnetic susceptibility (χ_M') versus frequency for **1c** (top) and **1o** (bottom) under H_{DC} = 0 Oe (left column) and H_{DC} = 1600 Oe (right column).

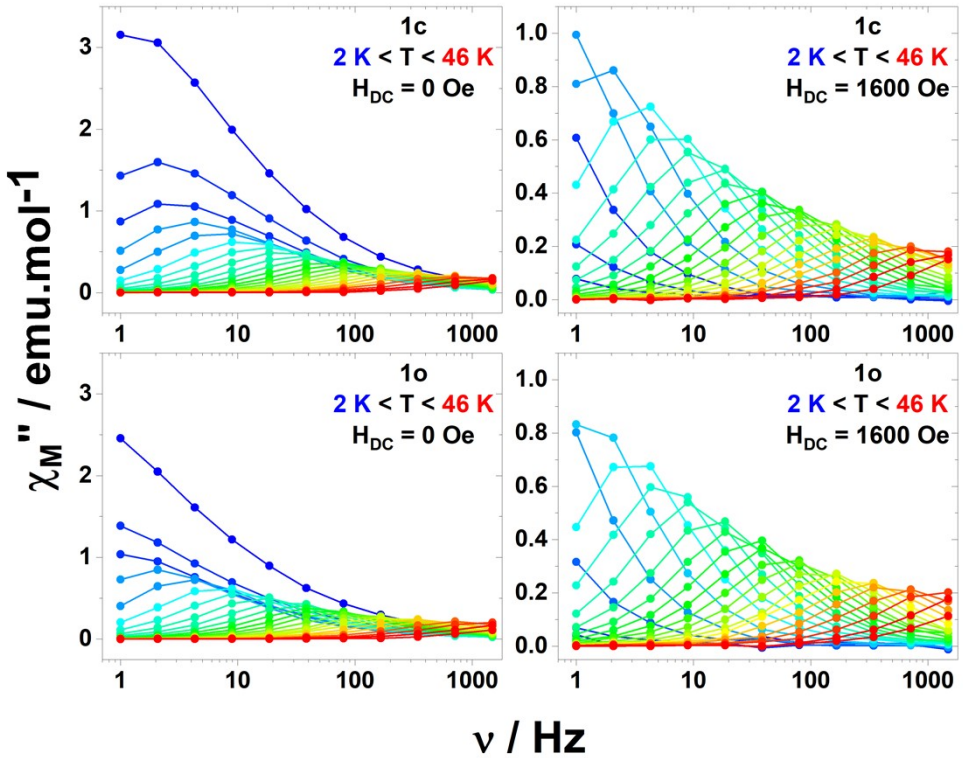

Figure S25. Out-of-phase molar magnetic susceptibility (χ_M'') versus frequency for **1c** (top) and **1o** (bottom) under H_{DC} = 0 Oe (left column) and H_{DC} = 1600 Oe (right column).

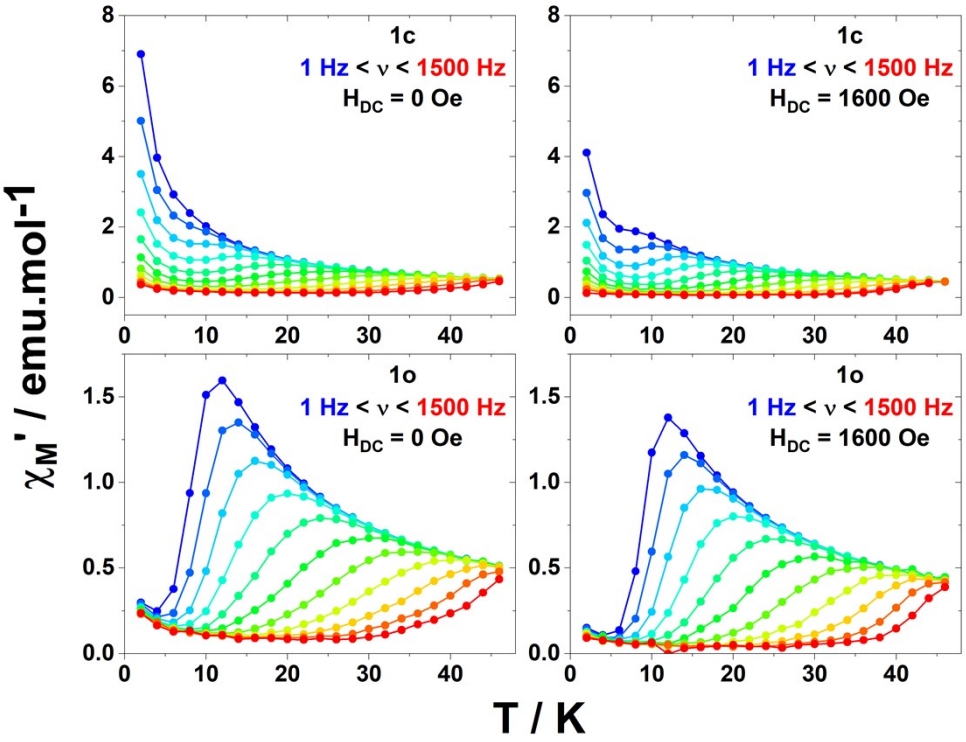

Figure S26. In-phase molar magnetic susceptibility (χ_M') versus temperature for **1c** (top) and **1o** (bottom) under H_{DC} = 0 Oe (left column) and H_{DC} = 1600 Oe (right column).

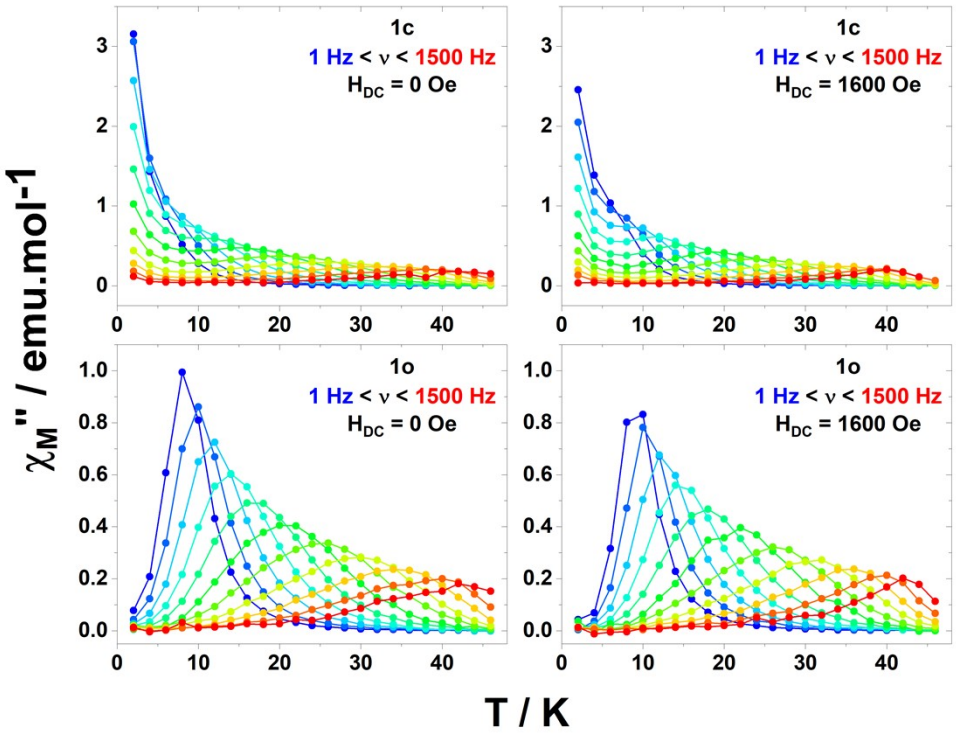

Figure S27. Out-of-phase molar magnetic susceptibility (χ_M'') versus temperature for **1c** (top) and **1o** (bottom) under H_{DC} = 0 Oe (left column) and H_{DC} = 1600 Oe (right column).

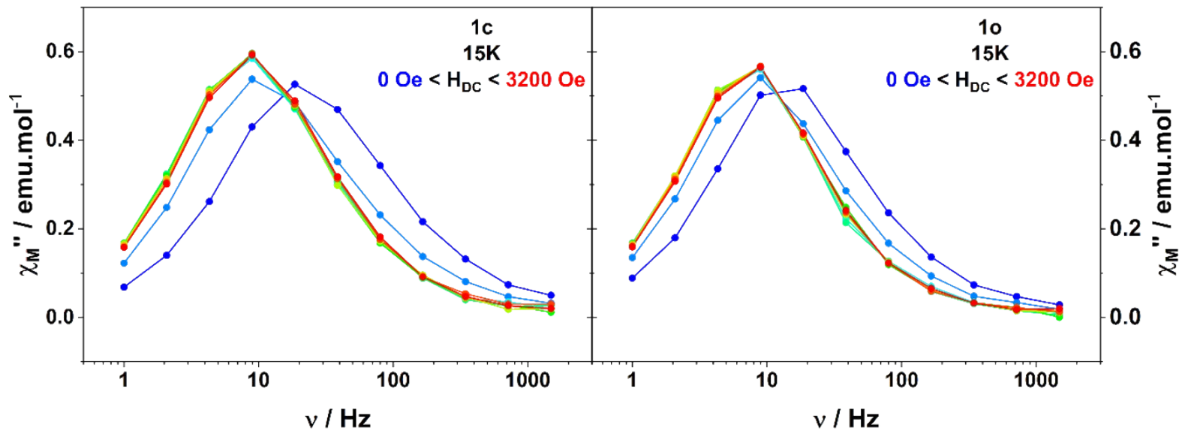

Figure S28. Out-of-phase magnetic susceptibility (χ_M'') versus frequency for **1c** (top) and **1o** (bottom).

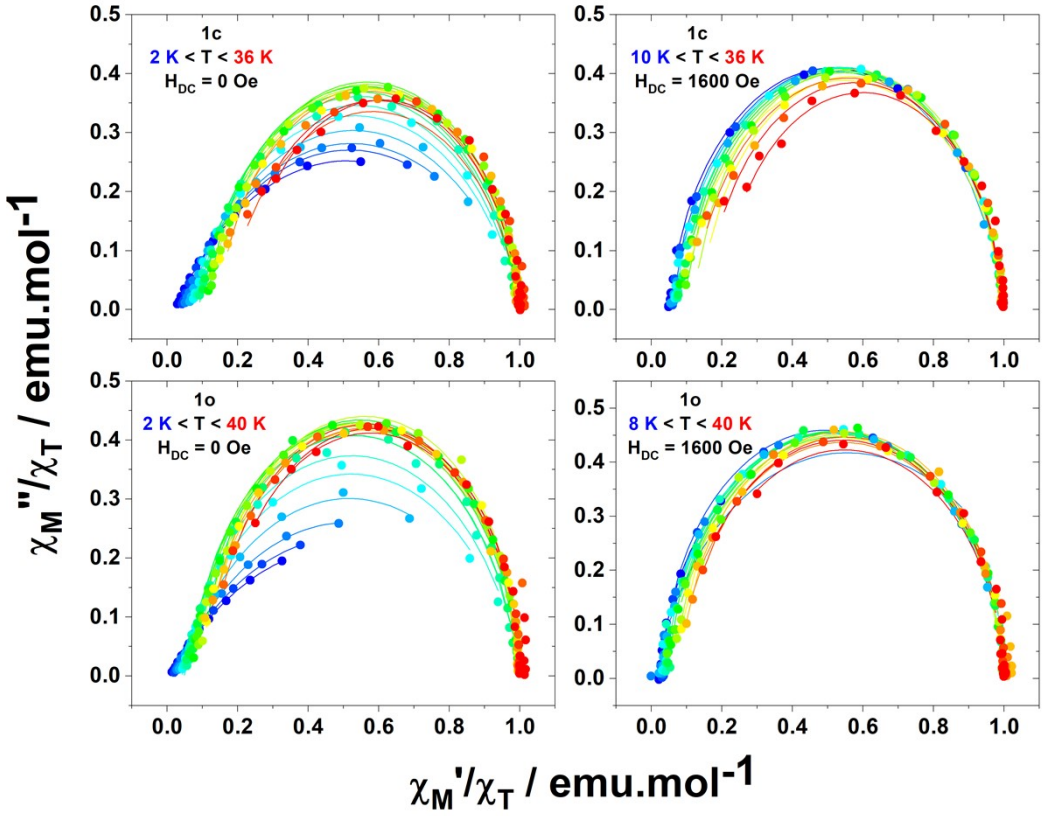

Figure S29. Cole-Cole plots normalized by the isothermal susceptibility (χ_T) for on **1c** (top) and **1o** (bottom) with H_{DC} = 0 Oe (left column) and H_{DC} = 1600 Oe (right column), with the best fits as full lines (see Table S12).

5. DFT and TD-DFT Study

Computational details. DFT geometry optimizations and TD-DFT excitation energy calculations were performed with Gaussian16.A03 using default algorithms, procedures, and convergence thresholds.[9] The ground-state geometries were optimized with the PBE0 hybrid functional[10-11] and we checked that the minimal structures were true minima (absence of an imaginary frequency) at the same level of theory. The "Stuttgart/Dresden" basis sets and effective core potentials were used to describe the yttrium atom,[1] while light atoms were described with SVP basis sets.[12] The first 50 monoelectronic excitations were calculated. Molecular orbitals were sketched using the Gabedit graphical interface.[13]

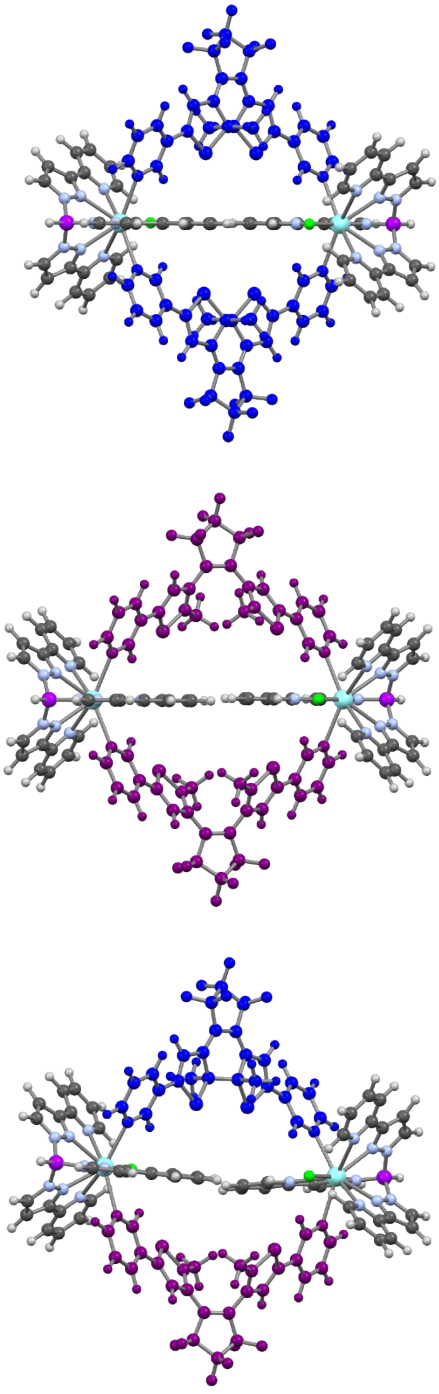

Figure S30. DFT optimized structure of $[(Y(Tp^{py})F)_2(L_c)_2]^{2+}$ (top), $[(Y(Tp^{py})F)_2(L_o)_2]^{2+}$ (middle) and $[(Y(Tp^{py})F)_2(L_o)(L_c)]^{2+}$ (bottom).

Table S14. TD-DFT calculated excitation energies (E_{ex}, nm), oscillator strength (f) and compositions of the main low-lying electronic transitions for $[(Y(Tp^{py})F)_2(L_c)_2]^{2+}$, $[(Y(Tp^{py})F)_2(L_o)_2]^{2+}$ and $[(Y(Tp^{py})F)_2(L_o)(L_c)]^{2+}$.

E_{ex}	f	Composition of the transition
$[(Y(Tp^{py})F)_2(L_c)_2]^{2+}$		
609	0.77	HOMO-1 – LUMO (48%) HOMO – LUMO+1 (52%)
371	0.19	HOMO – LUMO+6 (69%) HOMO-2 – LUMO (10%) HOMO-1 – LUMO+7 (8%)
$[(Y(Tp^{py})F)_2(L_o)_2]^{2+}$		
320	0.24	HOMO – LUMO+5 (38%) HOMO-1 – LUMO+4 (31%) HOMO-1 – LUMO+8 (15%)
314	0.57	HOMO – LUMO+1 (53%) HOMO-1 – LUMO (28%)
$[(Y(Tp^{py})F)_2(L_o)(L_c)]^{2+}$		
602	0.39	HOMO – LUMO (1.00)
320	0.16	HOMO-1 – LUMO+5 (36%) HOMO-1 – LUMO+8 (29%) HOMO-1 – LUMO+6 (10%)

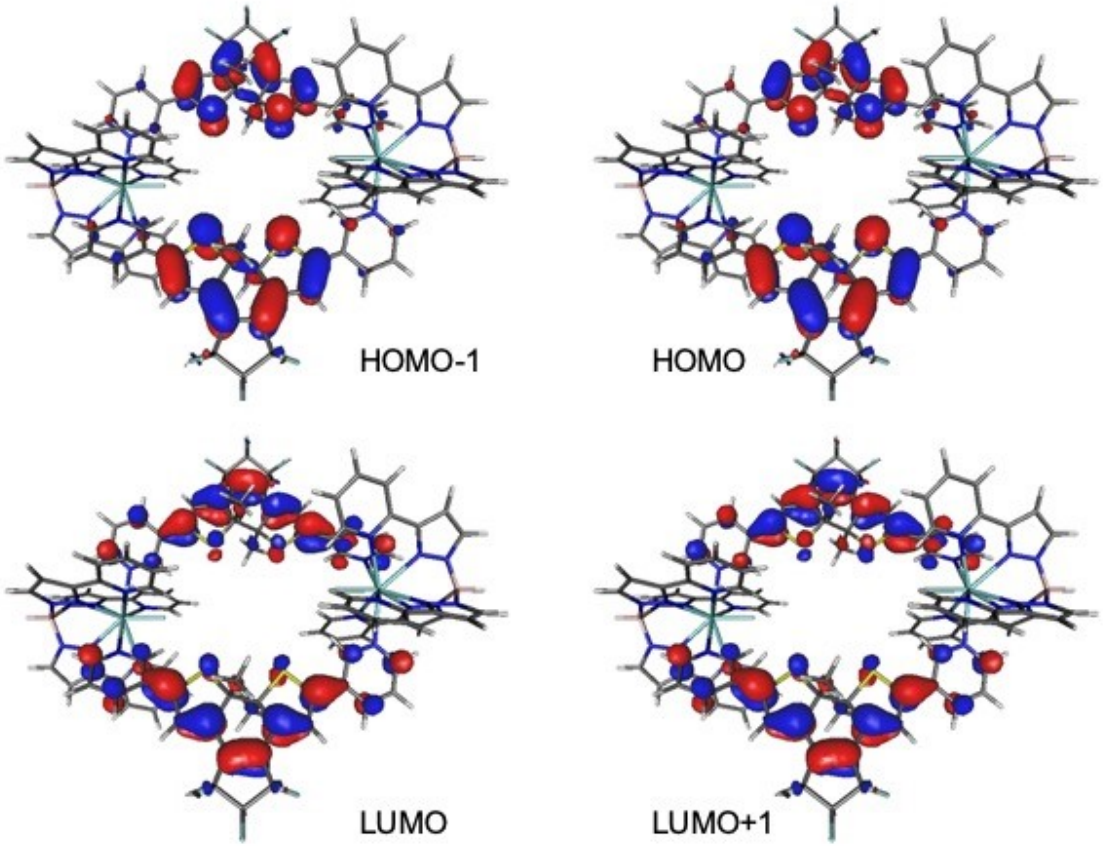

Figure S31. Frontier orbitals involved in the main low-lying transition for $[(Y(Tp^{py})F)_2(L_c)_2]^{2+}$.

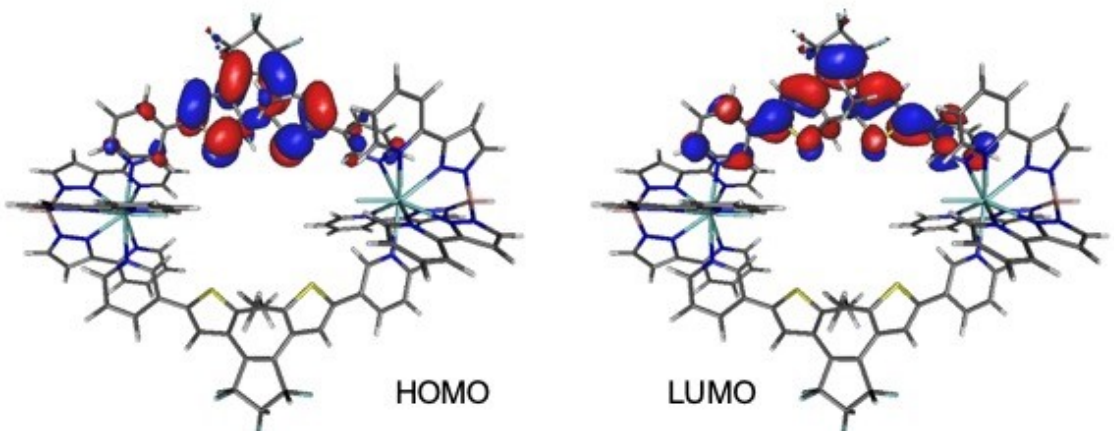

Figure S32. Frontier orbitals involved in the main low-lying transition for $[(Y(Tp^{py})F)_2(L_o)(L_c)]^{2+}$.

- **References:**

1. Norel, L. *et al.* A Terminal Fluoride Ligand Generates Axial Magnetic Anisotropy in Dysprosium Complexes. *Angew. Chemie - Int. Ed.* **2018**, **57**, 1933–1938 .

2. Wei, S. *et al.* Creating Coordination-Based Cavities in a Multiresponsive supramolecular gel. *Chem. - A Eur. J.* **2015**, **21**, 7418–7427.

3. CrysAlisPro 1.171.41.95a. (2021) Rigaku OD.

4. O.V. Dolomanov, L.J. Bourhis, R.J. Gildea, J.A.K. Howard, H. Puschmann. *J. Appl. Cryst.* **2009**, 42, 339-341.

5. G. M. Sheldrick, *Acta Cryst.*, **2015**, A71, 3-8.

6. G.M. Sheldrick, *Acta Cryst.*, **2015**, C71, 3-8.

7. P. v.d. Sluis and A.L. Spek, *Acta Cryst.* **1990** A46, 194-201.

8. A. L. Spek, *J. Appl. Cryst.* **2003**, 36, 7-13.

9. Frisch, M. J.; Trucks, G. W.; Schlegel, H. B.; Scuseria, G. E.; Robb, M. A.; Cheeseman, J. R.; Scalmani, G.; Barone, V.; Petersson, G. A.; Nakatsuji, H.; Li, X.; Caricato, M.; Marenich, A. V.; Bloino, J.; Janesko, B. G.; Gomperts, R.; Mennucci, B.; Hratchian, H. P.; Ortiz, J. V.; Izmaylov, A. F.; Sonnenberg, J. L.; Williams; Ding, F.; Lipparini, F.; Egidi, F.; Goings, J.; Peng, B.; Petrone, A.; Henderson, T.; Ranasinghe, D.; Zakrzewski, V. G.; Gao, J.; Rega, N.; Zheng, G.; Liang, W.; Hada, M.; Ehara, M.; Toyota, K.; Fukuda, R.; Hasegawa, J.; Ishida, M.; Nakajima, T.; Honda, Y.; Kitao, O.; Nakai, H.; Vreven, T.; Throssell, K.; Montgomery Jr., J. A.; Peralta, J. E.; Ogliaro, F.; Bearpark, M. J.; Heyd, J. J.; Brothers, E. N.; Kudin, K. N.; Staroverov, V. N.; Keith, T. A.; Kobayashi, R.; Normand, J.; Raghavachari, K.; Rendell, A. P.; Burant, J. C.; Iyengar, S. S.; Tomasi, J.; Cossi, M.; Millam, J. M.; Klene, M.; Adamo, C.; Cammi, R.; Ochterski, J. W.; Martin, R. L.; Morokuma, K.; Farkas, O.; Foresman, J. B.; Fox, D. J. Gaussian 16 Rev. A.03, Wallingford, CT, 2016.

10. Perdew, J. P.; Burke, K.; Ernzerhof, M., Generalized Gradient Approximation Made Simple. *Phys. Rev. Lett.* **1996**, 77 (18), 3865-3868.

11. Adamo, C.; Barone, V., Toward reliable density functional methods without adjustable parameters: The PBE0 model. *J. Chem. Phys.* **1999**, 110 (13), 6158-6170.

12. Dolg, M.; Stoll, H.; Preuss, H., A combination of quasi-relativistic pseudopotential and ligand-field calculations for lanthanoid compounds. *Theoretica Chimica Acta* **1993**, 85 (6), 441-450.

13. Allouche, A.-R., Gabedit—A graphical user interface for computational chemistry softwares. *J. Comput. Chem.* **2011**, 32 (1), 174-182.